Journal of Advanced Marine Engineering and Technology, Vol. 50, No. 1, pp. 1~15, 2026
J. Advanced Marine Engineering and Technology (JAMET)
https://doi.org/10.5916/jamet.2026.50.1.1

ISSN 2234-7925 (Print)
ISSN 2765-4796 (Online)
Original Paper

Flammability and limit oxygen concentration of hydrogen–methane counterflow diffusion flames: Effects of blending ratio and global strain rate

Juwon Park[1,†]

(Received February 23, 2026 ; Revised February 24, 2026 ; Accepted February 26, 2026)

Abstract: The increasing adoption of hydrogen-enriched fuels in maritime propulsion systems necessitates quantitative fire-safety criteria under leakage-driven, oxygen-lean environments. In nitrogen-inerted marine compartments, accidental release of hydrogen–methane mixtures may lead to diffusion flames whose stability is governed by the combined effects of oxygen concentration and flow-induced stretch. In this study, one-dimensional counterflow diffusion flame simulations were performed to systematically investigate the limit oxygen concentration (LOC) and extinction characteristics of hydrogen–methane blends with hydrogen fractions ranging from 50% to 100%. The effects of global strain rate, preferential diffusion, and radiative heat loss were examined using detailed chemical kinetics (GRI-Mech 3.0 and San Diego mechanisms). The LOC was found to increase monotonically with global strain rate for all blending ratios, indicating progressive narrowing of the flammability envelope under stronger stretch. At a fixed strain rate, hydrogen-rich mixtures exhibited lower LOC values, reflecting enhanced chemical robustness and wider intrinsic flammability. Radiation effects were shown to be negligible except in the very low-strain regime, where subtle transport–chemistry coupling influences near-extinction behavior. Detailed flame-structure analysis revealed a transition in extinction-side location: radiation-dominated oxidizer-side extinction at low strain and stretch-controlled fuel-side extinction at high strain. Methane addition modified this behavior through preferential diffusion and deficient-reactant transport effects. To unify extinction behavior across blending ratios, a hybrid non-dimensional extinction parameter combining the critical Karlovitz number and strain–diffusion scaling was introduced. When plotted against the Peclet number in log–log space, extinction data collapsed onto a single power-law trajectory over more than two orders of magnitude. This master extinction curve demonstrates that hydrogen–methane diffusion flame extinction can be described by a unified transport–chemistry scaling, largely independent of blending ratio in the high-stretch regime.

Keywords: Limit oxygen concentration, Hydrogen-methane, Global strain rate

1. Introduction

The global maritime industry is undergoing an unprecedented transition toward decarbonization in response to increasingly stringent international regulations. The International Maritime Organization (IMO) has adopted ambitious greenhouse gas (GHG) reduction strategies, including the Energy Efficiency Existing Ship Index (EEXI), Carbon Intensity Indicator (CII), and the long-term target of net-zero emissions by 2050 **[1]**. These regulatory frameworks have accelerated the development and deployment of alternative marine fuels, particularly hydrogen-based energy carriers and hydrogen-enriched natural gas systems **[2]**. In this transitional phase, blending hydrogen with methane is regarded as a technically feasible and infrastructure-compatible solution for reducing carbon intensity while maintaining operational reliability in marine engines and gas-fueled propulsion systems **[3][4]**.

Hydrogen blending into methane significantly alters combustion characteristics due to its high reactivity, low molecular weight, and small Lewis number **[5]**. Numerous studies have demonstrated that hydrogen addition increases laminar burning velocity, extends flammability limits, enhances radical production, and modifies flame structure **[6]**. In premixed combustion systems, preferential diffusion of hydrogen induces thermo-diffusive instabilities and cellular flame structures, leading to substantial variations in local temperature and species distribution **[7]**. In non-premixed configurations, particularly in counterflow

† Corresponding Author (ORCID: https://orcid.org/0000-0002-1944-5574): Ph. D. Candidate, Department of Marine System Engineering, Korea Maritime & Ocean University, 727, Taejong-ro, Yeongdo-gu, Busan 49112, Korea, E-mail: pjw6642@gmail.com, Tel: +51-410-4261

1 Ph. D. Candidate, Interdisciplinary Major of Maritime AI Convergence, National Korea Maritime & Ocean University, E-mail: pjw6642@gmail.com, Tel: +82-51-410-4261

diffusion flames, hydrogen addition modifies the interaction between strain rate, diffusion transport, and chemical kinetics, thereby altering extinction behavior and stability limits **[8]**.

Despite extensive investigations into hydrogen–methane combustion focusing on flame speed enhancement, pollutant formation, and thermoacoustic response, comparatively limited attention has been devoted to systematic evaluation of flammability limits and limit oxygen concentration (LOC) across the entire blending range from pure methane to pure hydrogen. From a marine safety perspective, such evaluation is critically important. Hydrogen possesses a significantly wider flammable range and lower ignition energy than methane, which may increase the risk of accidental ignition or explosion in confined engine rooms, fuel storage compartments, or ventilation ducts aboard vessels **[9]**. The safety design of gas-fueled ships therefore requires quantitative criteria for inerting and oxygen concentration control, especially under leakage or abnormal operating conditions.

In diffusion flame configurations, flame extinction is governed by the competition between chemical reaction time scales and flow-induced strain. The counterflow geometry has been widely adopted as a canonical configuration for investigating extinction limits because it provides a well-defined one-dimensional similarity structure and allows precise control of global strain rate **[10]**. In such strained systems, extinction can occur either due to excessive flame stretch at high strain rates or due to heat losses and weakened reaction intensity at low strain rates **[11]**. The introduction of hydrogen further complicates this balance by increasing reactivity while simultaneously enhancing differential diffusion effects. Consequently, the flammability limit and LOC are expected to depend not only on blending ratio but also on the imposed strain field **[12]**.

Accordingly, motivated by the urgent need to establish quantitative fire safety criteria for hydrogen-blended marine fuel systems, the present study focuses on the hydrogen-rich blending regime ranging from 50% to 100% hydrogen, where flammability enhancement and safety concerns become particularly pronounced. One-dimensional numerical simulations of hydrogen–methane counterflow diffusion flames are performed to evaluate flame stability characteristics under strained conditions representative of leakage-driven flow fields. Specifically, the combined effects of hydrogen blending ratio and global strain rate on flammability limits and limit oxygen concentration (LOC) are systematically examined. By constructing extinction maps and analyzing detailed flame structure variations, including temperature distribution and reactive species profiles, this study seeks to elucidate the coupled strain–diffusion–chemistry mechanisms governing extinction behavior in hydrogen-enriched mixtures. The ultimate objective is to provide physically grounded LOC criteria and stability boundaries that can support safety-oriented design and risk mitigation strategies for hydrogen-blended fuel systems in maritime environments.

2. Research Scope

The primary objective of this study is to establish quantitative operating criteria for a fire prevention system applied to a high-pressure hydrogen–methane blended fuel tank, with particular emphasis on hydrogen-rich mixtures ranging from 50% to 100% hydrogen. As summarized in **Figure 1**, hydrogen exhibits an exceptionally wide flammable range (4.0–75.0%), extremely low minimum ignition energy (approximately 0.018 mJ), and high auto-ignition temperature compared to conventional marine fuels such as methane and methanol **[13]**. Although methane possesses a relatively narrower flammable range and higher minimum ignition energy, the incorporation of hydrogen significantly enhances mixture reactivity and broadens the overall flammability envelope. Consequently, hydrogen-rich methane blends introduce elevated ignition sensitivity and increased risk of secondary fire in confined marine environments.

In contrast to previous studies where ambient pressure was treated as a controlling parameter, the present investigation focuses exclusively on two dominant variables relevant to leakage-driven fire scenarios in marine applications: hydrogen blending ratio and global strain rate, the latter representing the characteristic leakage velocity field. The global strain rate is adopted as a physically meaningful parameter that captures the coupling between

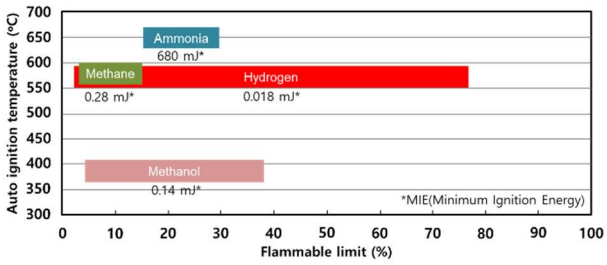

Figure 1: Comparative flammability limits (LFL–UFL), auto-ignition temperatures (AIT), and minimum ignition energies (MIE) of major alternative marine fuels

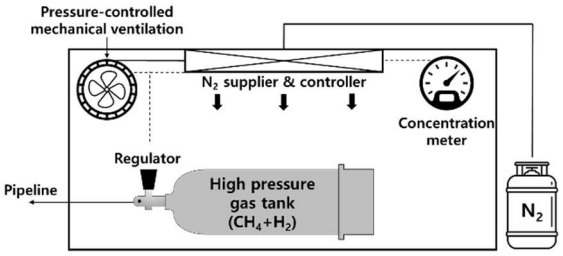

Figure 2: Conceptual design of the fire prevention system applied to a high-pressure hydrogen–methane storage tank, incorporating oxygen concentration monitoring, nitrogen supply, and pressure control mechanisms

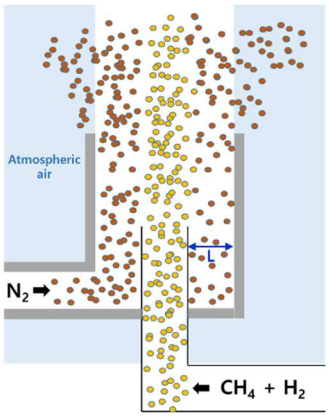

Figure 3: Coaxial ventilation structure for safe discharge of leaked hydrogen–methane mixtures, employing an outer nitrogen curtain flow to suppress air entrainment and mitigate secondary fire risk

flow-induced stretch and chemical reaction time scales in a counterflow diffusion configuration. By systematically varying hydrogen fraction within the hydrogen-rich regime and imposing a range of strain rates representative of accidental release conditions, the study aims to determine the limiting oxygen concentration (LOC) required to suppress ignition and flame propagation.

Figure 2 illustrates the conceptual fire prevention system proposed for the hydrogen–methane storage tank. The system integrates oxygen concentration monitoring, controlled nitrogen injection, and pressure management mechanisms to maintain the surrounding environment outside the flammability limits. Under normal operating conditions, the oxygen concentration within the enclosed compartment is regulated below the flammable threshold. Upon detection of abnormal leakage or pressure reduction within the fuel tank, nitrogen is rapidly supplied to reduce oxygen concentration and mitigate ignition risk.

Figure 3 presents the coaxial ventilation structure designed for emergency discharge of leaked hydrogen–methane mixtures. In this configuration, the inner duct releases the flammable gas, while the outer annulus supplies a nitrogen curtain flow that envelops the leaking jet. The nitrogen curtain serves to suppress air entrainment, delay mixing with ambient oxygen, and thereby minimize the possibility of secondary ignition outside the tank. This design concept is particularly critical for hydrogen-rich mixtures, where rapid diffusion and extremely low ignition energy can otherwise promote flashback or jet-fire formation.

To quantitatively define safe operating conditions for this integrated prevention system, the present study constructs LOC maps as functions of hydrogen blending ratio and global strain rate. By coupling detailed flame structure analysis with extinction criteria in a one-dimensional counterflow diffusion framework, the research seeks to elucidate the strain–diffusion–chemistry interactions governing ignition suppression in hydrogen-enriched methane mixtures.

3. Computational Method

3.1 Numerical Configuration and Boundary Conditions

To investigate extinction characteristics and limiting oxygen concentration (LOC) behavior of hydrogen–methane blended fuels under leakage-representative conditions, a one-dimensional counterflow diffusion flame configuration was employed, as schematically illustrated in **Figure 4**. The opposed-jet configuration has been extensively utilized as a canonical platform for examining flame structure, extinction limits, and strain–chemistry interactions due to its well-defined similarity solution and controllable strain field **[14][15]**.

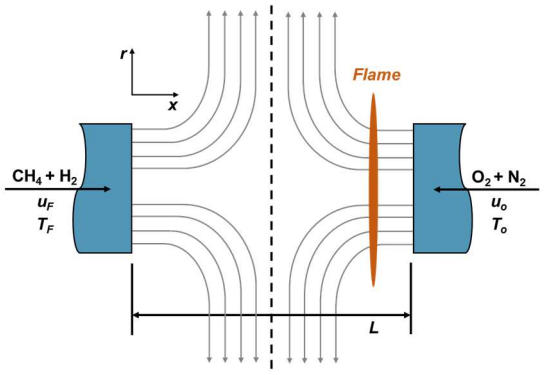

Figure 4: Schematic representation of the one-dimensional counterflow diffusion flame configuration employed for evaluating extinction behavior and limit oxygen concentration (LOC) of hydrogen–methane blended fuels

In the present configuration, the fuel stream and oxidizer stream are injected from two opposing nozzles, forming a stagnation plane between them. A diffusion flame is established in the vicinity of the oxidizer side, where the mixing layer supports chemical reaction between the counterflowing streams. Owing to the inherent one-dimensional similarity structure of the counterflow field, detailed transport and chemical kinetic effects can be resolved with high fidelity while maintaining computational efficiency, even when detailed reaction mechanisms are adopted.

The fuel stream consisted of hydrogen–methane mixtures with hydrogen fractions ranging from 50% to 100% on a molar basis, representing hydrogen-rich blending conditions relevant to marine fuel transition scenarios. The oxidizer stream was composed of $O_2 - N_2$ mixtures, where the oxygen mole fraction was systematically varied to determine extinction conditions. The oxygen concentration at the extinction point was defined as the limit oxygen concentration (LOC).

Both streams were introduced at 298 K and atmospheric pressure. Unlike previous investigations where ambient pressure was treated as a variable, the present study fixed the pressure at 1 atm to isolate the effects of blending ratio and flow-induced strain. The global strain rate was varied over a wide range to simulate different leakage intensities, specifically: 5, 10, 20, 30, 40, 50, 75, 100, 150, 500, 1000, and 1500 s^{-1}.

The global strain rate, a_g, is defined as **[16]**:

$$a_g = \frac{2u_O}{L}\left[1 + \frac{u_F}{u_O}\frac{\sqrt{\rho_F}}{\sqrt{\rho_O}}\right] \quad (1)$$

where u and ρ denote the axial velocity and density, respectively, and subscripts O and F refer to oxidizer and fuel streams. In this study, equal inlet velocities were imposed for both streams to ensure symmetric strain conditions. The nozzle separation distance L was fixed at 2 cm.

3.2 Chemical Kinetic Mechanisms and Radiation Modeling

To assess the sensitivity of extinction behavior and LOC prediction to chemical kinetics, two detailed reaction mechanisms were employed: GRI-Mech 3.0 and the San Diego mechanism **[17][18]**. GRI-Mech 3.0 has been extensively validated for methane and light hydrocarbon combustion, whereas the San Diego mechanism provides improved representation of hydrogen oxidation chemistry and high-temperature radical kinetics. Comparative analysis using both mechanisms enables evaluation of kinetic model dependency under hydrogen-rich blending conditions.

Radiative heat loss was incorporated using the optically thin radiation model **[19]**, accounting for contributions from major radiating species including CO_2, CO, CH_4, and H_2O. Since Planck-mean absorption coefficients (PMACs) for nitrogen-containing species are not directly available within the standard optically thin framework, PMAC values for relevant nitrogen species were obtained from the HITRAN 2008 spectroscopic database **[20][21]**. Inclusion of radiation effects is particularly important for capturing low-strain extinction behavior where heat loss mechanisms may influence flame stability.

All simulations were conducted under steady-state conditions using detailed transport properties. The LOC was determined by progressively reducing the oxygen mole fraction in the oxidizer stream until flame extinction occurred at each prescribed hydrogen blending ratio and global strain rate. Lastly, all simulations were performed using Chemkin-Ansys software **[22]**.

4. Computational Results

4.1 Flame Structure and Thermal Characteristics under Air Conditions

Under air conditions (X_O = 0.21), the variation of maximum flame temperature with global strain rate is shown in **Figure 5** for hydrogen blending ratios of 50%, 70%, and 100%. Since the analysis was conducted exclusively in the post-turning-point regime, only the descending branch of the classical C-curve is observed. In this high-strain region, flame extinction behavior is predominantly governed by stretch-induced weakening of reaction intensity rather than radiative heat loss.

As expected, the maximum flame temperature decreases monotonically with increasing global strain rate for all blending ratios. The increase in strain reduces the residence time of reactants within the reaction zone and compresses the preheat layer, thereby limiting radical accumulation and suppressing heat release. Consequently, thermal quenching becomes progressively dominant as the stretch intensity increases.

At moderate strain rates (a_g = 30 s^{-1}), the maximum flame temperature increases with hydrogen fraction, reflecting the higher reactivity and faster chain-branching kinetics of hydrogen-rich mixtures. However, at extremely high strain rates (a_g =1500 s^{-1}), a crossover behavior is observed, where the 70%

hydrogen mixture exhibits a slightly higher maximum temperature than the 100% hydrogen case. This non-monotonic trend suggests that under intense stretch conditions, flame structure is influenced not only by intrinsic chemical reactivity but also by differential diffusion effects and flame position shift.

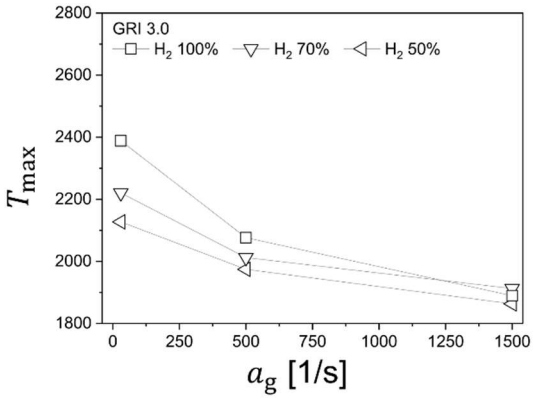

Figure 5: Maximum flame temperature versus global strain rate under air conditions (X_O = 0.21), showing the descending branch of the extinction curve

With increasing strain, the reaction zone moves toward the fuel side due to enhanced convective transport. In pure hydrogen flames, the high diffusivity of H_2 promotes deeper penetration toward the oxidizer side under moderate conditions, but under strong stretch, rapid radical leakage and insufficient residence time can suppress peak heat release. In contrast, the addition of methane introduces slower-diffusing species that tend to anchor part of the reaction zone closer to the fuel nozzle. This localized stabilization can partially compensate for stretch-induced weakening, resulting in a slightly higher maximum temperature at intermediate blending ratios.

Therefore, the observed crossover at high strain indicates a complex interplay between stretch intensity, differential diffusion, and reaction zone relocation. This behavior will be further clarified in **Figure 6** through detailed analysis of major species distributions and heat release rate (HRR) profiles along the axial direction.

Figure 6 presents the axial distributions of major species mole fractions and heat release rate (HRR) as a function of distance

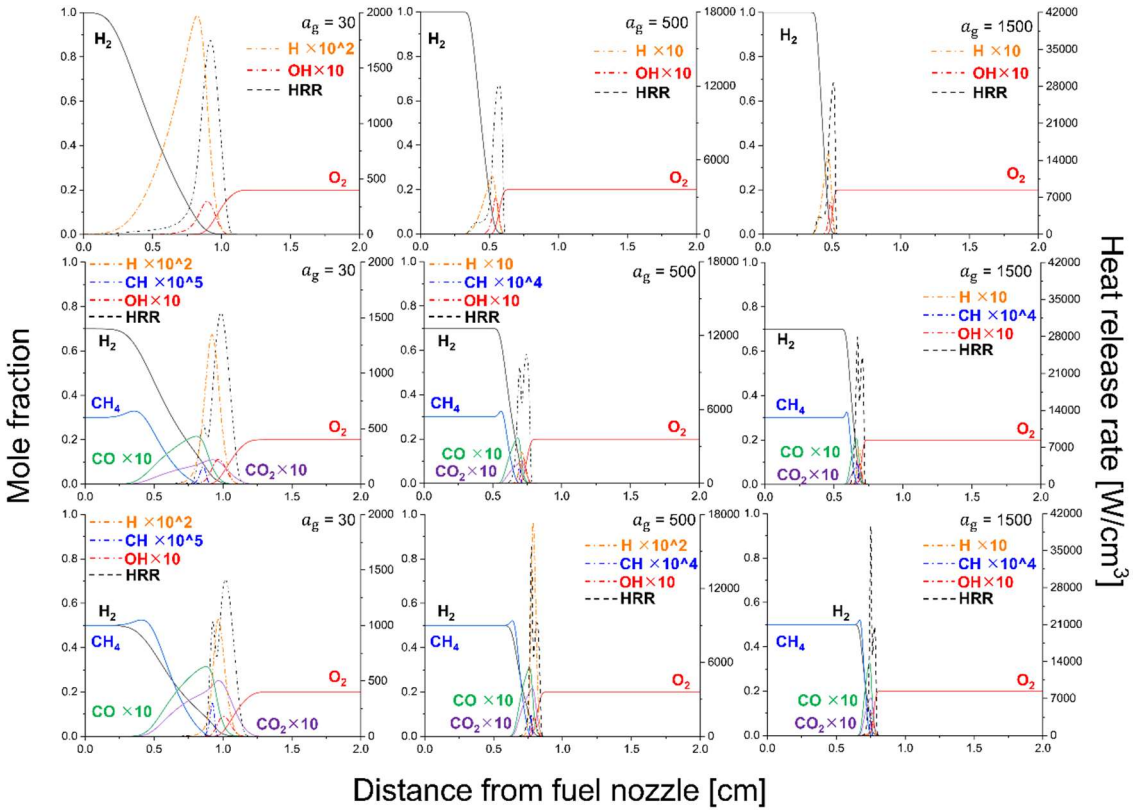

Figure 6: Axial distributions of mole fractions (left axis) of major species (H_2, CH_4, CO, CO_2, O_2, H, CH, OH) and heat release rate (HRR, right axis) as a function of distance from the fuel nozzle under air conditions (X_O = 0.21). The 3 × 3 matrix is arranged as follows: columns correspond to global strain rates of a_g = 30, 500, and 1500 s^{-1} from left to right, while rows represent hydrogen blending ratios of 100%, 70% (H_2/CH_4 = 70/30), and 50% (H_2/CH_4 = 50/50) from top to bottom

from the fuel nozzle under air conditions (X_O = 0.21). The left axis represents mole fractions of H_2, CH_4, CO ($\times 10$), CO_2 ($\times 10$), O_2, H ($\times 10^2$), CH ($\times 10^5$), and OH ($\times 10$), where the scaling factors are introduced solely to enhance visualization of minor species without altering their relative spatial trends. The right axis corresponds to the HRR. The spatial location of the HRR peak directly represents the flame position.

For the pure hydrogen case (100% H_2), the maximum HRR increases with increasing global strain rate. It should be noted that the right vertical scales differ among strain conditions, and therefore the absolute magnitude must be interpreted accordingly. The increase in peak HRR with strain is physically attributed to the enhanced reactant flux into the reaction zone; higher strain intensifies convective transport, thereby increasing the rate of reactant supply per unit time. Simultaneously, the flame position shifts toward the fuel side as strain increases. This relocation occurs because the enhanced oxidizer-side momentum compresses the reaction zone and reduces the residence time on the oxidizer side, forcing the stoichiometric surface to migrate toward the fuel stream in order to satisfy the local mixing balance.

At the HRR peak location, hydrogen and oxygen mole fractions intersect and rapidly approach zero, indicating that the flame sheet is formed where the reactants are nearly completely consumed. The OH radical profile closely follows the HRR distribution, confirming its role as a primary heat-release mediator. In contrast, the H radical concentration rises sharply in the region where hydrogen begins to decrease, reaching a maximum slightly upstream of the HRR peak and then rapidly diminishing as hydrogen is fully consumed. This behavior reflects the fast chain-branching kinetics of hydrogen oxidation, where H radicals are generated in the preheat and reaction zones but cannot be sustained once the fuel is depleted.

When methane is introduced (70% H_2/ 30% CH_4), the overall trend with strain remains similar: increasing strain elevates the peak HRR and shifts the flame toward the fuel side. However, a distinct double-peak structure emerges in the HRR distribution. This feature can be interpreted in terms of differential mass diffusion between hydrogen and methane. At 1 atm and 300 K, the binary diffusion coefficient of H_2 in air is approximately 0.87 cm^2/s, whereas that of CH_4 in air is about 0.23 cm^2/s **[23]**, indicating that hydrogen diffuses roughly three times faster than methane. Because methane diffuses more slowly, it is consumed closer to the fuel side, forming the first HRR peak. Hydrogen, with its higher diffusivity, penetrates further toward the oxidizer side before being consumed, producing the second HRR peak. The mole fraction of hydrogen correspondingly decreases closer to the oxidizer side compared to methane.

At low strain (a_g = 30 s^{-1}), the hydrogen-dominated second peak is more pronounced due to sufficient residence time for radical accumulation and chain branching. As strain increases, the separation between the consumption locations of hydrogen and methane diminishes because strong stretch compresses the reaction zone. Under such conditions, the two HRR peaks progressively merge and may even reverse in relative magnitude. The first peak, initially associated with methane oxidation, becomes strengthened by overlapping hydrogen reactions, reflecting enhanced radical coupling under intense stretch.

Despite the dual HRR structure, the OH radical distribution consistently exhibits a single dominant peak. This suggest that the spatial generation zones of OH induced by hydrogen and methane oxidation substantially overlap, even though their fuel-consumption zones are separated. Therefore, OH serves as an integrated marker of total heat release rather than distinguishing between the two fuel-specific reaction fronts.

The presence of methane also leads to the formation of CO and CO_2. Both species appear downstream of the methane consumption region and extend toward the oxidizer side. CO_2 penetrates further into the oxidizer side than CO, consistent with progressive oxidation ($CO \rightarrow CO_2$) in oxygen-rich regions. An interesting feature is that the methane mole fraction exhibits a slight increase relative to its initial normalized value near the early reaction zone. This does not indicate physical production of methane but arises from the definition of mole fraction as a normalized quantity:

$$X_{\mathrm{CH4}} = \frac{n_{\mathrm{CH4}}}{\sum n_{\mathrm{i}}} \tag{2}$$

If other species such as H_2 or radicals decrease more rapidly in the denominator (total moles), the normalized methane mole fraction may appear to increase slightly even when its absolute molar concentration remains nearly constant. This effect is particularly noticeable in regions where hydrogen is preferentially consumed or diffuses away faster than methane.

For the equimolar case (50% H_2/ 50% CH_4), similar double-peak behavior is observed, but the structural separation becomes more pronounced. As methane dilution increases at fixed strain, the overall HRR profile becomes thinner. This can be related to

differences in thermal diffusivity. At 300 K and 1 atm, the thermal diffusivity of hydrogen is approximately $1.6\times10^{-4}m^2/s$, whereas that of methane is roughly $2.3\times10^{-5}m^2/s$ **[24]**, indicating that hydrogen possesses nearly an order-of-magnitude higher thermal diffusivity. Consequently, hydrogen promotes broader preheat regions and more distributed heat transport, whereas methane favors more localized heat release.

At a fixed global strain rate, increasing methane content results in a systematic shift of the dominant HRR peak toward the oxidizer side. This behavior should not be interpreted solely as a consequence of methane's slower molecular diffusion, but rather as a global mixture-transport effect associated with preferential diffusion and reactant deficiency.

As methane fraction increases, the initial hydrogen concentration correspondingly decreases while the binary diffusion coefficients of hydrogen and oxygen remain essentially unchanged. Under these conditions, the mixture becomes increasingly hydrogen-deficient relative to oxygen in the vicinity of the reaction zone. Because hydrogen possesses a significantly smaller molecular weight and larger mass diffusivity, the preferential diffusion effect becomes more pronounced in lean hydrogen conditions. In other words, the effective Lewis number of the deficient reactant decreases, enhancing preferential diffusion toward the oxidizer stream **[7]**.

This intensified preferential diffusion shifts the stoichiometric surface and the peak heat-release region toward the oxidizer side. From a similarity-solution perspective in counterflow diffusion flames, flame position is determined by the balance between convective transport and differential diffusion of the deficient reactant. When hydrogen becomes the limiting species due to methane dilution, its enhanced diffusion relative to oxygen alters the local mixture fraction gradient and redefines the location where stoichiometric balance is achieved.

Consequently, the entire reaction structure—including the HRR peak—moves toward the oxidizer side as methane content increases. This shift reflects a global transport-chemistry coupling effect rather than a purely local two-peak interaction. The observed behavior therefore indicates that, under fixed strain conditions, flame positioning is governed by the increasing dominance of preferential diffusion of the deficient reactant rather than by methane's intrinsic diffusivity alone.

4.2 Limit Oxygen Concentration and Near-Extinction Flame Structure under Varying Strain Rates

In practical marine applications, accidental leakage from a high-pressure hydrogen–methane storage tank is likely to occur within an enclosed fuel preparation or storage compartment. As introduced in Section 2, such compartments are typically designed to be inerted by systematic nitrogen purging, such that the leaked fuel jet is exposed not to atmospheric air but to an environment with a substantially reduced oxygen mole fraction. Moreover, during emergency discharge, the coaxial ventilation concept (nitrogen curtain flow) further suppresses ambient air entrainment into the leaking stream, sustaining a low-oxygen surrounding over a wide range of leakage intensities. Under these conditions, fire prevention and mitigation are governed by whether the oxygen concentration remains below the limit oxygen concentration (LOC) required for extinction. Therefore, quantitative LOC mapping as a function of global strain rate—serving as a physically meaningful surrogate for leakage-driven stretch—is essential for defining safe operating boundaries and for interpreting near-extinction flame structures relevant to hydrogen-enriched marine fuel systems.

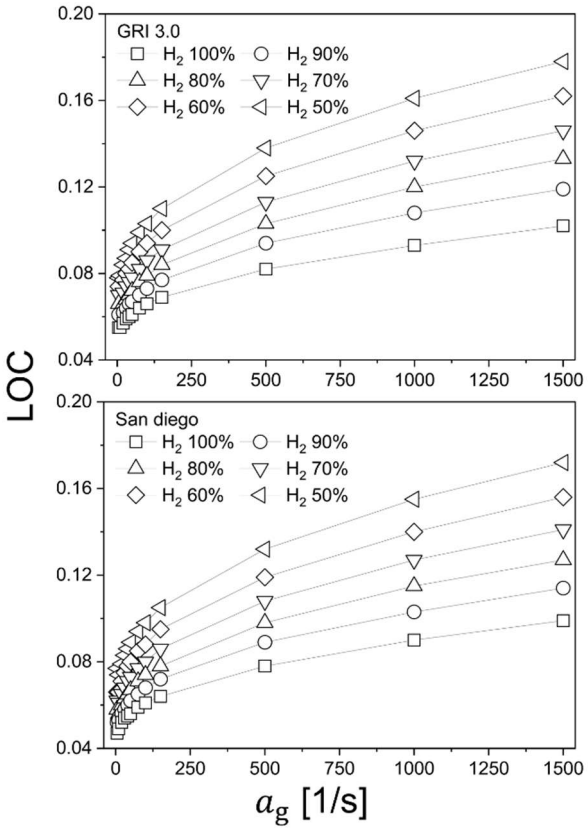

Figure 7: Strain-dependent limit oxygen concentration (LOC) for hydrogen–methane counterflow diffusion flames with hydrogen fractions of 50%, 70%, and 100%; comparison between (a) GRI-Mech 3.0 and (b) San Diego chemical kinetic mechanisms

Figure 7 presents the LOC as a function of global strain rate for hydrogen blending ratios of 50%, 70%, and 100%. Results obtained using GRI-Mech 3.0 are shown in the upper panel, while those computed using the San Diego mechanism are shown in the lower panel. For all blending ratios, the LOC increases monotonically with increasing global strain rate. This trend indicates that the flammability envelope narrows under stronger stretch, such that extinction can be induced at progressively higher oxygen concentrations as the strain field intensifies. Physically, increasing strain reduces the convective–diffusive residence time available for reactants to mix and react, compresses the preheat layer, and enhances scalar dissipation in the reaction zone. As a result, radical buildup and heat-release intensity are increasingly suppressed, rendering the flame more susceptible to stretch-induced quenching; consequently, less severe oxygen depletion is required to extinguish the flame at higher strain rates.

At a fixed strain rate, increasing hydrogen fraction leads to a lower LOC, implying enhanced flammability and greater resistance to extinction in hydrogen-rich mixtures. This behavior is consistent with the intrinsically broader flammability limits of hydrogen compared to methane and its higher chemical reactivity, which sustains chain-branching and heat release even under oxygen-lean conditions. In other words, as the mixture becomes more hydrogen-dominant, the critical oxygen level required to suppress ignition and flame stabilization decreases, thereby demanding more stringent inerting requirements from a safety-design perspective.

A comparison between the two mechanisms reveals that the overall LOC trends are qualitatively and quantitatively similar, indicating limited kinetic-model sensitivity for the present hydrogen-rich diffusion-flame extinction problem under the tested conditions. Nevertheless, the San Diego mechanism yields slightly higher LOC values than GRI-Mech 3.0, suggesting a modest tendency to overpredict extinction susceptibility (i.e., to require a marginally higher oxygen concentration for extinction) relative to GRI-Mech 3.0. The primary motivation for adopting the San Diego mechanism, despite the small discrepancy, is its capability to consistently enable radiation heat-loss modeling to be switched on and off within the numerical framework. Given that the two mechanisms provide nearly identical LOC predictions, the San Diego mechanism offers a robust baseline for isolating radiative heat-loss effects without introducing significant kinetic bias.

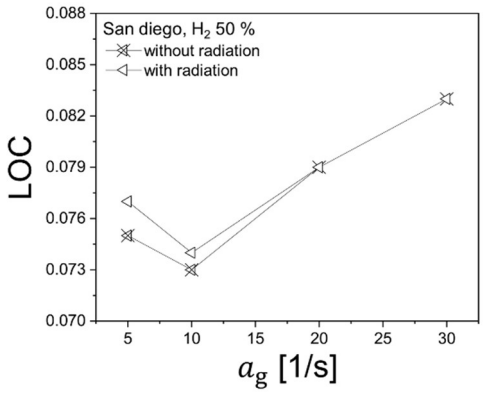

Figure 8: Comparison of limit oxygen concentration (LOC) with and without radiative heat loss at low global strain rates (a_g = 5–30 s^{-1}) for a 50% hydrogen–50% methane counterflow diffusion flame, highlighting near-extinction behavior under weak stretch conditions

Accordingly, the following **Figure 8** examines the LOC behavior at low strain rates with and without radiative heat loss, where heat-loss mechanisms may become non-negligible near extinction. This comparison is intended to clarify whether radiative cooling measurably alters the LOC boundary in hydrogen–methane diffusion flames under oxygen-lean, near-extinction conditions relevant to nitrogen-inerted marine compartments.

Figure 8 presents the variation of limit oxygen concentration (LOC) at low global strain rates (a_g = 5, 10, 20, and 30 s^{-1}) for the 50% hydrogen–50% methane mixture. Results obtained with and without radiative heat loss are compared in order to isolate the influence of thermal radiation on extinction behavior under weak stretch conditions.

At moderate low strain rates (a_g = 20, and 30 s^{-1}), the inclusion or exclusion of radiative heat transfer has a negligible effect on the predicted LOC. The two curves nearly overlap, indicating that, in this strain regime, extinction is still primarily governed by stretch–chemistry interaction rather than by heat-loss mechanisms. The preheat layer remains sufficiently compressed, and the reaction intensity is mainly controlled by scalar dissipation rather than radiative cooling.

However, for $a_g \leq 10$ s^{-1}, a measurable difference emerges. When radiative heat loss is neglected, the predicted LOC becomes slightly lower, indicating enhanced flame robustness. Physically, removing radiative cooling artificially elevates the local flame temperature, promotes radical accumulation, and increases the net heat-release rate. Consequently, a lower oxygen concentration is required to extinguish the flame. This behavior

is consistent with classical low-strain extinction theory, in which radiative heat loss competes with chemical heat release when convective stretch becomes weak **[8]**.

A particularly interesting feature is the non-monotonic behavior observed around a_g = 10 s^{-1}. The strain rate a_g = 10 s^{-1} appears to correspond to a turning point in the low-strain regime. As strain decreases from 20 to 10 s^{-1}, the LOC decreases as expected due to reduced stretch intensity. However, when the strain rate is further reduced to a_g = 5 s^{-1}, the LOC increases again, indicating that extinction becomes possible at higher oxygen concentrations despite the weaker stretch.

From a combustion-theory perspective, such behavior may be interpreted as a transition between stretch-dominated and transport-dominated extinction regimes. At extremely low strain, the flame thickness increases substantially, and the reaction zone becomes more sensitive to heat-loss mechanisms and preferential diffusion effects. In hydrogen–methane mixtures, differential diffusion between hydrogen (high diffusivity) and methane (lower diffusivity) can alter the local stoichiometric balance when convective transport is weak. Under these conditions, the deficient reactant distribution and local mixture fraction gradients may shift in a manner that reduces radical accumulation efficiency, even though stretch intensity is low. This can lead to partial weakening of the reaction zone and an apparent increase in LOC at very low strain.

Alternatively, the observed LOC increase at a_g = 5 s^{-1} may be associated with enhanced diffusive–radiative coupling in thicker flame structures, where increased residence time allows cumulative radiative cooling to compete more effectively with chemical heat release. Because hydrogen–methane mixtures contain CO_2 and H_2O as radiating species, radiative losses may become non-negligible in sufficiently broadened reaction zones.

At present, while these interpretations are physically plausible, definitive identification of the dominant mechanism requires further analysis of local Damköhler number, Lewis number variation, and detailed radical transport budgets. Therefore, the anomalous LOC rise observed at a_g = 5 s^{-1} is tentatively attributed to complex differential diffusion effects in hydrogen–methane co-combustion and will be investigated in future work through parametric sensitivity analysis and extended transport modeling.

Overall, Figure 8 demonstrates that radiative heat loss exerts only a secondary influence on LOC for hydrogen–methane diffusion flames, except in the very low strain regime where transport–chemistry coupling becomes increasingly subtle.

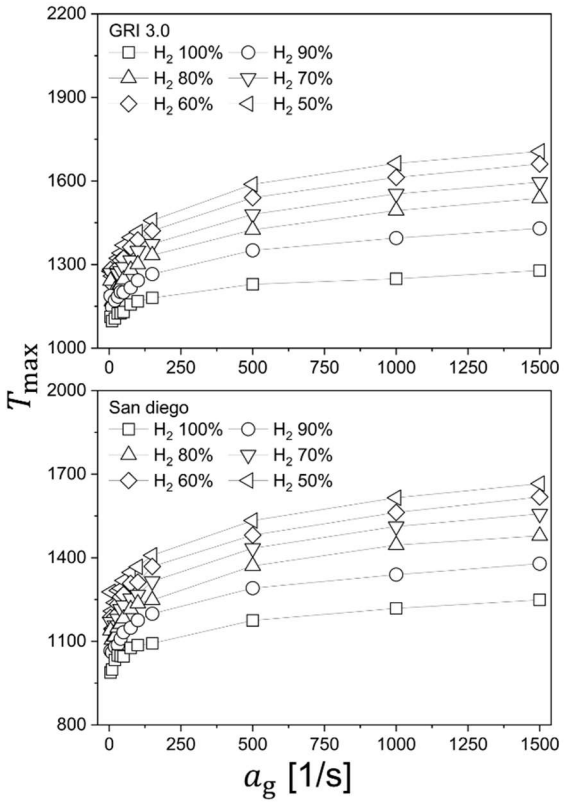

Figure 9: Strain-dependent adiabatic flame temperature at the extinction limit (LOC condition) for hydrogen–methane counterflow diffusion flames with varying hydrogen blending ratios (50–100% H_2); comparison of predictions using (a) GRI-Mech 3.0 and (b) the San Diego mechanism

These findings confirm that, under nitrogen-inerted marine conditions, extinction boundaries are primarily governed by stretch intensity and preferential diffusion, with radiation playing a limited but non-negligible role near the weak-stretch limit.

Figure 9 presents the adiabatic flame temperature evaluated at the corresponding LOC conditions for each global strain rate. In other words, the plotted temperature represents the thermal state of the flame immediately adjacent to extinction. The upper panel shows results obtained using GRI-Mech 3.0, while the lower panel corresponds to calculations based on the San Diego mechanism.

As shown in the figure, the variation of adiabatic flame temperature exhibits a trend that is fully consistent with the LOC behavior presented in **Figure 7**. Specifically, as the global strain rate increases, the adiabatic flame temperature at the extinction limit increases monotonically. This indicates that under stronger stretch conditions, extinction occurs at progressively higher thermal states. Physically, increasing strain intensifies scalar

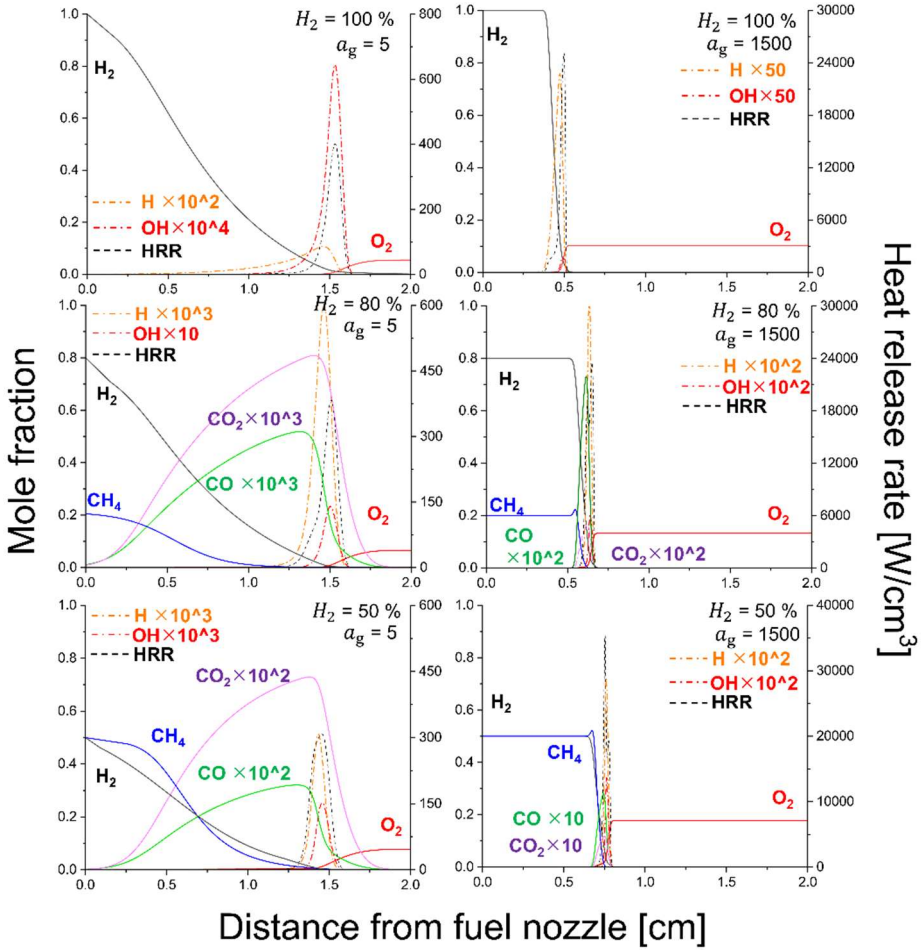

Figure 10: Axial distributions of mole fractions (left axis) of major species (H_2, CH_4, CO, CO_2, O_2, H, CH, OH) and heat release rate (HRR, right axis) as a function of distance from the fuel nozzle under air conditions (X_O = 0.21). The 3 × 3 matrix is arranged as follows: columns correspond to global strain rates of a_g = 30, 500, and 1500 s^{-1} from left to right, while rows represent hydrogen blending ratios of 100%, 70% (H_2/CH_4 = 70/30), and 50% (H_2/CH_4 = 50/50) from top to bottom

dissipation and reduces the effective Damköhler number, thereby requiring a higher local temperature (i.e., stronger reaction intensity) to sustain flame stabilization at the threshold of extinction.

At a fixed strain rate, an interesting behavior is observed: as the hydrogen blending ratio increases, the adiabatic flame temperature evaluated at the LOC condition becomes relatively lower. This trend should not be interpreted as a contradiction to the intrinsic property that hydrogen exhibits higher adiabatic flame temperatures than methane under stoichiometric air conditions. Instead, it reflects the fact that the present temperatures correspond to near-extinction states rather than freely propagating stoichiometric flames.

In hydrogen-rich mixtures, enhanced chain-branching kinetics and preferential diffusion effects allow the flame to remain stabilized even at lower thermal intensities under oxygen-deficient conditions. Consequently, hydrogen-enriched flames can survive at lower adiabatic flame temperatures before reaching extinction, whereas methane-rich mixtures require comparatively higher temperatures to maintain sufficient radical production near the extinction boundary. Therefore, the observed reduction in near-extinction adiabatic temperature with increasing hydrogen fraction is a manifestation of increased chemical robustness rather than reduced intrinsic reactivity.

A comparison between GRI-Mech 3.0 and the San Diego mechanism reveals that the predicted adiabatic flame temperatures differ by approximately 100 K, with the San Diego mechanism yielding slightly higher extinction-limit temperatures. Despite this quantitative difference, both mechanisms exhibit nearly identical monotonic trends with respect to strain rate and hydrogen blending ratio. This consistency further confirms that the

extinction behavior of hydrogen–methane counterflow diffusion flames in the present parameter space is governed primarily by transport–chemistry coupling rather than by strong kinetic-model dependency.

Figure 10 presents the axial distributions of major species mole fractions (H_2, CH_4, CO, CO_2, O_2, H, CH, and OH) and heat release rate (HRR) under LOC conditions, corresponding to flame structures immediately adjacent to extinction. The left column represents the low-strain condition (a_g = 5 s−1), while the right column corresponds to the high-strain condition (a_g = 1500 s−1), and the rows denote hydrogen blending ratios of 100%, 80%, and 50%, respectively. Since all cases are evaluated at LOC, the flame structures shown here represent marginally sustainable reaction states where the balance between chemical heat release and transport losses is critically poised.

For the pure hydrogen flame, a clear transition in extinction-side location is observed as the strain rate varies. At low strain (a_g = 5 s−1), extinction occurs closer to the oxidizer side. In this regime, the effective Damköhler number is relatively large because chemical time scales remain shorter than flow time scales. Consequently, extinction is not governed by stretch but rather by cumulative heat-loss mechanisms, primarily radiative cooling. Under low stretch, the reaction zone is relatively thick, allowing radiation to act over an extended preheat region. The oxidizer-side portion of the flame, being exposed to lower fuel concentration and weaker radical replenishment, becomes more susceptible to temperature reduction, leading to extinction near the oxidizer boundary. In contrast, at high strain (a_g = 1500 s−1), the Damköhler number decreases significantly due to intense stretch and enhanced scalar dissipation. Under these conditions, extinction becomes stretch-controlled: the reaction zone is compressed, residence time is reduced, and radical buildup is inhibited. The stoichiometric surface shifts toward the fuel side, and insufficient chemical time for hydrogen oxidation results in extinction occurring preferentially near the fuel boundary. Thus, for pure hydrogen, the extinction location transitions from oxidizer-side (radiation-dominated, high Damköhler number) to fuel-side (stretch-dominated, low Damköhler number) as strain increases.

When methane is introduced (80% H_2 / 20% CH_4), the overall extinction-side transition with strain remains qualitatively similar, but notable differences emerge in the detailed structure. Unlike the fully burning air-condition flames discussed previously, no distinct double-peak HRR structure is observed under LOC conditions. This indicates that near extinction, the reaction intensity is insufficient to sustain spatially separated methane- and hydrogen-dominated heat-release zones. Instead, the weakened reaction collapses into a single marginal reaction layer. At low strain, decreasing hydrogen content causes the extinction location to move gradually from the oxidizer side toward the fuel side. This behavior can be interpreted in terms of radiation-dominated extinction: methane addition increases the concentration of radiatively active species such as CO_2 and H_2O, thereby enhancing emissive heat loss. The strengthened radiative cooling reduces thermal robustness of the flame core and shifts the weakest reaction region toward the fuel side relative to the pure hydrogen case. At high strain, however, the trend reverses: as hydrogen fraction decreases, the extinction location shifts slightly from the fuel side toward the oxidizer side. Under strong stretch conditions, extinction is controlled primarily by scalar dissipation and deficient-reactant transport. The addition of methane reduces the overall hydrogen concentration while the binary diffusion coefficients of hydrogen and oxygen remain essentially unchanged. As hydrogen becomes increasingly deficient under oxygen-lean LOC conditions, preferential diffusion effects are intensified. Because hydrogen possesses significantly higher mass diffusivity than methane, its preferential transport toward the oxidizer stream becomes more dominant, modifying the local mixture fraction gradient and shifting the location where stoichiometric balance can be sustained. Consequently, the extinction boundary moves toward the oxidizer side as hydrogen content decreases under high strain. For the equimolar mixture (50% H_2 / 50% CH_4), the same qualitative tendencies are observed, but the transport–chemistry coupling becomes more pronounced. At low strain (a_g = 5 s−1), increasing methane dilution further enhances radiative heat loss due to higher CO_2 and H_2O formation, reinforcing radiation-controlled extinction and driving the extinction location progressively toward the fuel side. Conversely, at high strain (a_g = 1500 s−1), the reduced hydrogen fraction strengthens the deficient-reactant preferential diffusion effect, resulting in a systematic migration of the extinction location toward the oxidizer side. Therefore, the extinction position under LOC is determined by two competing mechanisms whose dominance depends on the strain regime: radiation-induced thermal imbalance at low stretch and stretch–preferential diffusion coupling at high stretch.

4.3 Flame Extinction Curve

To establish a generalized extinction scaling applicable to hydrogen-methane blended diffusion flames, a hybrid non-dimensional parameter was introduced as:

$$\psi = Ka_{\mathrm{crit}}\left(\frac{a_g \alpha}{S_L^2}\right) \tag{3}$$

where the critical Karlovitz number is defined as $Ka_{\mathrm{crit}} = S_L/u_f$ **[25][26]**. Here, a_g denotes the global strain rate, S_L is the laminar burning velocity evaluated under the corresponding LOC condition, u_f is the inlet flow velocity, and α represents the thermal diffusivity.

The extinction parameter ψ was then examined as a function of the Peclet number,

$$Pe = \frac{Lu_f}{\alpha} \tag{4}$$

which characterizes the relative magnitude of convective transport to thermal diffusion **[27]-[29]**.

Figure 11 presents the extinction data in a log–log representation, where both axes are expressed in logarithmic scale. Remarkably, the extinction points corresponding to all hydrogen blending ratios collapse onto a nearly linear trajectory over more than two orders of magnitude in Peclet number. This linear behavior in log–log space indicates the existence of a clear power-law relationship of the form,

$$\psi = 10^{1.52} Pe^{-0.84} \tag{5}$$

where the exponent n remains approximately constant across the entire blending range from 50% to 100% hydrogen.

The emergence of a single power-law trend demonstrates that the extinction behavior of hydrogen–methane diffusion flames can be described by a unified scaling that integrates stretch intensity, chemical reactivity, and transport properties.

Although the proposed extinction parameter does not explicitly contain a Lewis number term, preferential diffusion effects are inherently embedded through S_L and the transport properties. The laminar burning velocity is strongly influenced by mixture composition and effective Lewis number, particularly in hydrogen-rich mixtures where differential diffusion significantly modifies flame structure, radical transport, and local reaction intensity. Consequently, preferential diffusion effects are indirectly incorporated into the extinction scaling via their impact on S_L, Ka_{crit}, and the associated transport–chemistry coupling.

In the low-Pe regime, corresponding to weak convection and relatively strong diffusive transport, the extinction parameter attains larger values and exhibits greater sensitivity to mixture composition. This region reflects the residual influence of heat-loss mechanisms and preferential diffusion effects near the LOC condition.

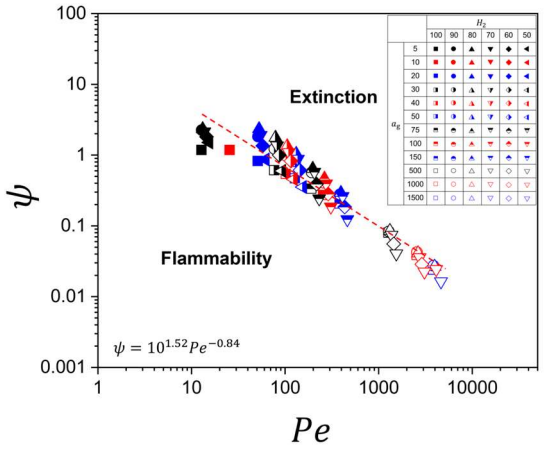

Figure 11: Hybrid extinction parameter (ψ) at flame extinction versus Peclet number for all tested hydrogen–methane blending conditions in this study

As Peclet number increases, representing progressively stronger convection and higher global strain rates, the data converge tightly onto the linear decay line. In this regime, extinction is predominantly governed by the competition between flow-induced stretch and chemical time scales, consistent with the classical scaling relation.

$$a_g \sim \frac{S_L^2}{\alpha} \tag{6}$$

The power-law collapse indicates that, despite substantial variations in laminar burning velocity and thermal diffusivity among hydrogen-rich and methane-diluted mixtures, the extinction boundary is ultimately controlled by a single composite parameter linking convective transport to reaction–diffusion balance.

Physically, the log–log linearity signifies a self-similar transition from diffusion-influenced extinction at low Peclet numbers to stretch-dominated extinction at high Peclet numbers. The absence of significant deviation among blending ratios in the high-Pe region confirms that mixture-dependent preferential diffusion becomes secondary once convective–chemical time-scale competition dominates.

4. Conclusion

This study established quantitative extinction and inerting criteria for hydrogen–methane blended fuels under oxygen-lean conditions representative of nitrogen-inerted marine

compartments. One-dimensional counterflow diffusion flame simulations were conducted for hydrogen-rich mixtures (50–100% H_2) to determine the limit oxygen concentration (LOC), near-extinction flame structure, and generalized extinction scaling over a wide range of global strain rates. Two detailed kinetic mechanisms (GRI-Mech 3.0 and San Diego) were employed to assess model sensitivity and to isolate radiative heat-loss effects. Under air conditions, the maximum flame temperature exhibited the descending branch of the classical extinction curve beyond the turning point, confirming that the examined regime is governed primarily by stretch-induced weakening. The crossover behavior observed at extremely high strain highlights that, even in hydrogen-dominant mixtures, flame response can be influenced by differential diffusion and reaction-zone relocation when residence time becomes critically limited. Species and heat-release profiles further demonstrated that global strain rate controls both the reactant flux and the flame location, while methane addition introduces additional transport–chemistry complexity through preferential diffusion and altered deficient-reactant balance.

Under LOC conditions relevant to nitrogen-purged environments, the LOC increased monotonically with global strain rate for all blending ratios, indicating progressive narrowing of the flammability envelope under stronger stretch. At a fixed strain rate, increasing hydrogen fraction consistently reduced the LOC, implying that hydrogen-enriched mixtures can sustain combustion at lower oxygen levels and therefore require more stringent inerting for safety. The comparison between GRI-Mech 3.0 and San Diego revealed nearly identical LOC trends, with only minor quantitative offsets; this agreement supports robust LOC prediction for hydrogen-rich counterflow diffusion flames within the present parameter space. Radiation was found to exert a secondary influence on LOC except in the very low-strain regime, where a non-monotonic LOC response suggested subtle coupling among radiative cooling, flame thickening, and mixture-transport effects; this anomalous behavior warrants further investigation via detailed budget analyses (e.g., local Damköhler number, Lewis-number variation, and radical transport).

Near-extinction flame-structure analysis clarified that the extinction-side location depends on the dominant loss mechanism. At low strain, extinction occurs closer to the oxidizer side, consistent with radiation-assisted weakening in thicker flames, whereas at high strain, extinction shifts toward the fuel side due to stretch-controlled suppression of reaction intensity and reduced residence time. Methane addition modified the extinction location in a strain-dependent manner, reflecting the competition between heat-loss sensitivity at weak stretch and preferential-diffusion-driven transport imbalance at strong stretch.

Finally, a generalized extinction characterization was achieved by introducing a hybrid non-dimensional extinction parameter ψ that combines the critical Karlovitz number with strain–diffusion scaling. When plotted against the Peclet number on log–log axes, extinction data for all blending ratios collapsed onto a near-linear trajectory over more than two orders of magnitude, indicating a clear power-law relationship. This master extinction curve demonstrates that hydrogen–methane diffusion flame extinction can be described by a unified transport–chemistry scaling, with mixture-dependent effects becoming secondary in the high-stretch regime.

Acknowledgement

This work was supported by Basic Science Research Program through the National Research Foundation of Korea (NRF) funded by the Ministry of Education (No.2021R1I1A3061305).

Author Contributions

Conceptualization, J. Park; Methodology, J. Park; Software, J. Park; Formal Analysis, J. Park; Investigation, J. Park; Resources, J. Park; Data Curation, J. Park; Writing-Original Draft Preparation, J. Park; Writing-Review & Editing, J. Park; Visualization, J. Park; Supervision, J. Park; Project Administration, J. Park; Funding Acquisition, J. Park.

References

[1] IMO, Revised GHG strategy for international shipping, International Maritime Organization, London, UK, 2023.

[2] H. H. Cho, V. Strezov, and T. J. Evans, “A review on global warming potential, challenges and opportunities of renewable hydrogen production technologies,” Sustainable Materials and Technologies, vol. 35, pp. e00567, 2023.

[3] X. Zhang, N. P. Myhrvold, Z. Hausfather, and K. Caldeira, “Climate benefits of natural gas as a bridge fuel and potential delay of near-zero energy systems,” Applied Energy, vol. 167, pp. 317-322, 2016.

[4] M. Levi, “Climate consequences of natural gas as a bridge fuel,” Climatic Change, vol. 118, pp. 609–623, 2013.

[5] C. K. Law, Combustion Physics, Cambridge University Press, New York, 2006.

[6] M. Ilbas, A. P. Crayford, I. Yılmaz, P. J. Bowen, and N. Syred, “Laminar-burning velocities of hydrogen–air and hydrogen–methane–air mixtures: an experimental study,” International Journal of Hydrogen Energy, vol. 31, pp. 1768–1779, 2006.

[7] M. Matalon, “Intrinsic flame instabilities in premixed and nonpremixed combustion,” Annual Review of Fluid Mechanics, vol. 39, pp. 163–191, 2007.

[8] H. Y. Wang, W. H. Chen, and C. K. Law, “Extinction of counterflow diffusion flames with radiative heat loss and nonunity Lewis numbers,” Combustion and Flame, vol. 148, pp. 100–116, 2007.

[9] I.C.S., “International code of safety for ships using gases or other low-flashpoint fuels (IGF code),” International Maritime Organization, 2017.

[10] H. Tsuji, “Counterflow diffusion flames,” Progress in Energy and Combustion Science, vol. 8, pp. 93–119, 1982.

[11] C. J. Sung, J. B. Liu, and C. K. Law, “Structural response of counterflow diffusion flames to strain rate variations,” Combustion and Flame, vol. 102, pp. 481–492, 1995.

[12] J. Jeon and S. J. Kim, “Recent progress in hydrogen flammability prediction for the safe energy systems,” Energies, vol. 13, pp. 6263, 2020.

[13] Y. H. Chung, W. -J. Lee, J. Kang, and S. H. Yoon, “Fire safety evaluation high-pressure ammonia storage systems,” Energies, vol. 15, pp. 520, 2022.

[14] R. J. Kee, J. A. Miller, G. H. Evans, and G. Dixon-Lewis, “A computational model of the structure and extinction of strained, opposed-flow premixed methane–air flames,” Proceedings of the Combustion, vol. 22, pp. 1479–1494, 1989.

[15] V. Giovangigli and M. D. Smooke, “Extinction of strained premixed laminar flames with complex chemistry,” Combustion Science and Technology, vol. 53, pp. 23–49, 1987.

[16] H. K. Chelliah, C. K. Law, T. Ueda, M. D. Smooke, and F. A. Williams, “An experimental and theoretical investigation of the dilution, pressure, and flow field effects on the extinction condition of methane–air–nitrogen diffusion flames,” Symposium (International) on Combustion, vol. 23, pp. 503–511, 1991.

[17] G. P. Smith, D. M. Golden, M. Frenklach, N. W. Moriarty, B. Eiteneer, M. Goldenberg, C. T. Bowman, R. K. Hanson, S. Song, W. C. Gardiner Jr., V. V. Lissianski, and Z. Qin, “GRI-Mech 3.0,” 1999. Available: http://combustion.berkeley.edu/gri-mech/index.html.

[18] Mechanical and Aerospace Engineering (Combustion Research) University of California at San Diego, “Chemical-Kinetic Mechanisms for Combustion Applications”, 2014. Available: http://combustion.ucsd.edu.

[19] R. S. Barlow, A. N. Karpetis, J. H. Frank, and J. Y. Chen, “Scalar profiles and NO formation in laminar opposed-flow partially premixed methane–air flames,” Combustion and Flame, vol. 127, pp. 2102-2118, 2001.

[20] M. F. Modest, Radiative Heat Transfer, 3rd ed., Academic Press, New York, NY, USA, 2013.

[21] L. S. Rothman, I. E. Gordon, A. Barbe, D. C. Benner, P. F. Bernath, M. Birk, V. Boudon, L. R. Brown, A. Campargue, J.-P. Champion, K. Chance, L. H. Coudert, V. Dana, V. M. Devi, S. Fally, J.-M. Flaud, R. R. Gamache, A. Goldman, D. Jacquemart, I. Kleiner, N. Lacome, W. J. Lafferty, J.-Y. Mandin, S. T. Massie, S. N. Mikhailenko, C. E. Miller, N. Moazzen-Ahmadi, O. V. Naumenko, A. V. Nikitin, J. Orphal, V. I. Perevalov, A. Perrin, A. Predoi-Cross, C. P. Rinsland, M. Rotger, M. Šimečková, M. A. H. Smith, K. Sung, S. A. Tashkun, J. Tennyson, R. A. Toth, A. C. Vandaele, and J. Vander Auwera, “The HITRAN 2008 molecular spectroscopic database,” Journal of Quantitative Spectroscopy and Radiative Transfer, vol. 110, pp. 533–572, 2009.

[22] ANSYS chemkin-pro, 2021.

[23] Transport Property Evaluation Website, Colorado State University Bioanalytical Microfluidics Program Chemical and Biological Engineering, Available: http://navier.engr.colostate.edu/code/code-2/index.html, Accessed September 30, 2019.

[24] P. J. Linstrom, and W. G. Mallard, “NIST chemistry webbook-standard reference database number 69”, 2025. Available: https://webbook.nist.gov/chemistry/.

[25] S. H. Chung, D. H. Chung, C. Fu, and P. Cho, “Local extinction karlovitz number for premixed flames,” Combustion and Flame, vol. 106, pp. 515–520, 1996.

[26] E. S. Cho, S. H. Chung, and T. K. Oh, “Local karlovitz numbers at extinction for various fuels in counterflow premixed flames,” Combustion Science and Technology, vol. 178, pp. 1559–1584, 2006.

[27] D. Bradley, R. A. Hicks, M. Lawes, C. G. W. Sheppard, and P. Cho, “The measurement of laminar burning velocities and Markstein numbers for iso-octane-air and iso-octane-n-heptane-air mixtures at elevated temperatures and pressures

in an explosion bomb," Combustion and Flame, vol. 115, pp. 126–144, 1998.

[28] D. Bradley, C. G. W. Sheppard, R. Woolley, D. A. Greenhalgh, and R. D. Lockett, "The development and structure of flame instabilities and cellularity at low Markstein numbers in explosions," Combustion and Flame, vol. 122, pp. 195–209, 2000.

[29] D. Bradley and C. M. Harper, "The development of instabilities in laminar explosion flames," Combustion and Flame, vol. 99, pp. 562–572, 1994.